Universal Scaling, Entanglements, and Knots of Model Chain Molecules

Katerina Foteinopoulou, Nikos Ch. Karayiannis,* and Manuel Laso
Institute for Optoelectronics and Microsystems (ISOM), Universidad Politécnica de Madrid (UPM), José Gutiérrez Abascal 2, 28006 Madrid, Spain

Martin Kröger
Polymer Physics, Department of Materials, ETH Zürich, Wolfgang-Pauli-Strasse 10, CH-8093 Zürich, Switzerland

Marc L. Mansfield
Department of Chemistry and Chemical Biology, Stevens Institute of Technology, Hoboken, New Jersey 07079, USA
(Received 16 August 2008; revised manuscript received 30 October 2008; published 30 December 2008)

By identifying the maximally random jammed state of freely jointed chains of tangent hard spheres we are able to determine the distinct scaling regimes characterizing the dependence of chain dimensions and topology on volume fraction. Calculated distributions of (i) the contour length of the primitive paths and (ii) the number of entanglements per chain agree remarkably well with recent theoretical predictions in all scaling regimes. Furthermore, our simulations reveal a hitherto unsuspected connection between purely intramolecular (knots) and intermolecular (entanglements) topological constraints.

DOI: 10.1103/PhysRevLett.101.265702 PACS numbers: 61.20.Ja, 02.10.Kn, 64.70.Q−, 64.75.Gh

Since Bernal's pioneering work almost half a century ago [1], a great deal of experimental, theoretical, and simulation effort has been devoted to the investigation of random packings of single spheres and other nonsymmetric hard-body objects, especially in the vicinity of the configuration referred to nowadays as the maximally random jammed (MRJ) state [2–4]. MRJ is defined as the state in which the most sensitive measure of order parameter is minimized among all statistically homogeneous and isotropic jammed structures [3]. In practice, as the MRJ state is approached the ability of hard spheres to move (''rattle'' [3] and ''flip'' [5] for monoatomic and chain systems, respectively) without incurring overlaps declines precipitously. Regarding random assemblies of chains of hard spheres, connectivity endows them with a rich physical behavior. The problem of densely packed polymers is of vital importance in thermodynamics, biology, phase transitions, glassy state, colloids, granular media, combinatorics, and perturbation theory. Recently, the computational challenge of determining the MRJ state could be solved, albeit for short chains only [5]. Thus, universal scaling, and asymptotic behavior in the infinite chain length (N) limit, as predicted by Edwards [6] and de Gennes [6] could only be conjectured.

In this Letter we determine, through extensive simulations, the MRJ state for strongly entangled freely jointed chains of tangent hard spheres (where bond length is fixed and equal to sphere diameter), deep in the asymptotic regime. This MRJ state is determined by means of large scale [$O(10^{11})$ steps], off-lattice, Monte Carlo simulations using a suite of powerful importance sampling, chain-connectivity altering algorithms [7] on a number of bulk systems ranging from 100 chains of $N = 12$ to 54 chains of $N = 1000$. Preliminary tests on cells of different sizes revealed the absence of system size effects on all calculated properties.

We show that, within statistical uncertainty, hard-sphere chains reach their MRJ state at the same volume fraction (φ) as single spheres, $\varphi^{\mathrm{MRJ}} \approx 0.638 \pm 0.004$, irrespective of chain length. The question is thus settled that neither chain length nor the tangency constraint of connectivity hinder random packing of chains with respect to assemblies of single spheres. This alone is an important result, but to understand it, we need to further analyze the underlying structure, i.e., chain stiffness and topology.

To achieve these additional goals we employ state-of-the-art geometrical algorithms to extract the amount of intermolecular (entanglements) and intramolecular (knots) topological constraints from the atomistic configurations. Entanglements and the corresponding primitive path (PP) networks lie at the heart of modern theories of polymer dynamics [6,8]. Analytical, mean field treatments have yielded crucial insights into the physics and rheology of polymeric fluids [9]. As a consequence of the desire to enrich such approaches with atomistic information, starting from the work of Everaers *et al.* [10] the development of algorithms for the determination of entanglements is proceeding at a frantic pace [11], with different approaches converging to a unified picture, as discussed in [12]. We adopt the efficient $Z1$ algorithm [13], which has advantages compared to the original ''annealing'' approach of [10]. The PP of a chain immersed in a sea of obstacles is the shortest path connecting the chain ends that does not violate the topological constraints imposed on it, and whose length strictly and continuously decreases during minimization. For a multichain system the PP is the short-

est multiple disconnected path. The $Z1$ algorithm provides the complete path including information about sphere index belonging to kinks (nodes), from which we extract the PP contour length L_{PP}, the number of entanglements (interior kinks) Z, their location, and the entanglement spacing N_e, defined as the number of hard spheres between two successive entanglements. By covering, through extensive Monte Carlo simulations, the whole density range for random hard-sphere chain packings ($0 \leq \varphi \leq \varphi^{MRJ}$) we are able to explore the effect of volume fraction on the stiffness of the parent chain (through the characteristic ratio C_n) and of the primitive path (through the step length of the primitive path b_{PP}). These quantities are defined as $C_n \equiv \langle R^2 \rangle/(N-1)/b_0^2$ and $b_{PP} \equiv \langle L_{PP} \rangle/(N-1)$, respectively, where $\langle R^2 \rangle$ is the mean square end-to-end distance, b_0 is the bond length (equal to the sphere diameter), and $\langle L_{PP} \rangle$ is the mean PP contour length.

As clearly shown in Fig. 1, regarding chain dimensions we identify four distinct scaling behaviors as φ increases, confirming the following theoretical expectations about the existence and ranges of regimes [14] denoted as "dilute" ($0 \leq \varphi \leq \varphi^{*,semi}$, $\varphi^{*,semi} \simeq N^{-0.764}$ [6]), "semidilute" ($\varphi^{*,marg} \simeq \varphi^{MRJ}/2 \simeq 0.32$ [15]), "marginal" ($\varphi^{*,marg} \leq \varphi \leq \varphi^{*,conc}$, $\varphi^{*,conc} \simeq 0.59$ [15]), and "concentrated" ($\varphi^{*,conc} \leq \varphi \leq \varphi^{MRJ}$). The corresponding exponents and crossover densities appear insensitive to chain length. We find the scaling exponents for C_n in the dilute, semidilute, marginal, and concentrated regimes to be equal to 0.0 ± 0.1, -0.23 ± 0.003, -1.0 ± 0.1, and 0.0 ± 0.1, respectively. Our values are in perfect agreement with available theoretical predictions and experimental findings of 0.0 (dilute) [6,16], -0.23 (semidilute) [6,14], -1.0 (marginal) [15], and 0.0 (concentrated) [14–16].

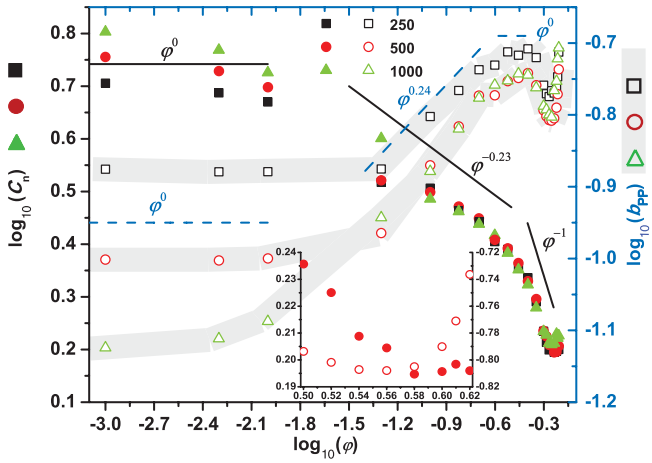

FIG. 1 (color). Characteristic ratio C_n of chains (left axis, filled symbols) and the step length of the primitive path b_{PP} (right axis, open symbols) both versus volume fraction φ. Lines with characteristic slopes are drawn as a guide to the eye. Inset: Zoom into the marginal and concentrated regimes of the 500-sphere chain system. Crossover volume fractions are discussed in the text part.

Additionally, numerical estimates for the crossover densities between concentration regimes ($\varphi^{*,marg} \simeq 0.32$ and $\varphi^{*,conc} \simeq 0.59$) support recently derived values obtained by monitoring the microscopic mechanisms of correlated fluctuations of φ and C_n in a semigrand canonical ensemble via a graph theoretical proof [15]. Our present findings constitute the first numerical determination of the static scaling exponents, as well as of the prefactors *not* captured by scaling theories, in the marginal and concentrated regimes. It is remarkable how faithfully the full range of expected behaviors is reproduced by this simplest possible molecular model, which emphasizes its value as a statistical mechanics workbench. Figure 1, besides displaying with unprecedented clarity the four concentration regimes regarding the behavior of chain dimensions, provides further information on the corresponding scaling of the underlying PP contour length. Here, the density dependence is quite a bit more complicated as the marginal regime is further split into three different subdomains. The obtained scaling regimes and the corresponding exponents n of b_{PP} can be summarized as (I) $0 \leq \varphi \leq \varphi^{*,semi}$, $n = 0.0 \pm 0.1$, (II) $\varphi^{*,semi} \leq \varphi \leq \varphi^{*,marg}$, $n = 0.23 \pm 0.05$, (III) $\varphi^{*,marg} \leq \varphi \leq 0.45$, $n = 0.0 \pm 0.1$, (IV) $0.45 \leq \varphi \leq 0.52$, $n = -0.70 \pm 0.15$, (V) $0.52 \leq \varphi \leq \varphi^{*,conc}$, $n = 0.0 \pm 0.1$, and (VI) $\varphi^{*,conc} \leq \varphi \leq \varphi^{MRJ}$, $n = 3.4 \pm 0.4$. At low concentration, regimes I and II of b_{PP} coincide with the ones of C_n. However, in the semidilute regime (II) the mild reduction of chain dimensions is accompanied by a small increase in PP size as shown by the almost opposite values of the two scaling exponents. Interestingly, the average PP length is sharply amplified ($n \approx 3.4$) in the concentrated regime (where chain dimensions remain unaltered) closely related to the increase in the entanglement density, as will be shown below. Scaling behaviors for PP-related quantities have been recently discussed for loosely to tightly entangled polymers [17].

The contour length L_{PP} is the primary quantity characterizing PPs with its definition-free statistics being also independent of the applied topological algorithm as documented in numerous simulation works [11,12]. Consequently, the theoretical prediction of L_{PP} statistics has drawn considerable scientific attention. Very recently, Khaliullin and Schieber [18] proposed an analytic expression for the cumulative probability of the primitive path length $P_c(L_{PP})$, based on a thermodynamically consistent slip-link model with the parameters being the number of Kuhn steps in the chain, N_K, and β which is approximately equal to the average number of Kuhn steps per entanglement strand, $\langle N_e \rangle$. Accordingly, $P_c(L_{PP})$ is defined as [18]

$$P_c(L_{PP}) = \{\mathrm{erf}[w(L_{PP} - L_{PP}^{mp})/L_{PP}^{mp}] + \mathrm{erf}(w)\}/[1 + \mathrm{erf}(w)],$$
$$w \equiv \sqrt{\nu^* N_K/\beta}, \quad (1)$$

where L_{PP}^{mp} is the most probable value for L_{PP} and ν^* is calculated through

$$\nu^* \cong \beta(L_{\mathrm{PP}}^{\mathrm{mp}})^2/[2N_K(\langle L_{\mathrm{PP}}^2\rangle - \langle L_{\mathrm{PP}}\rangle L_{\mathrm{PP}}^{\mathrm{mp}})]. \quad (2)$$

Our simulation findings for $P_c(L_{\mathrm{PP}})$ are in excellent agreement with these theoretical predictions over the whole density range as we show in Fig. 2 (inset) for the $N = 1000$ hard-sphere system. As the increase of both L_{PP} and b_{PP} is nonmonotonic with φ, cf. Fig. 1, the same holds for the distributions $P_c(L_{\mathrm{PP}})$. For $\varphi \geq 0.10$ the modified parameter ν^* oscillates around a plateau value of 1.07 ± 0.15 (data not visualized) which is very close to $\nu^* \simeq 1$ predicted in [18], and well below the random walk result, $\nu = 3/2$. This successful comparison demonstrates further the predictive power of the proposed slip-link model for chain systems from semidilute fluids to polymeric solids near the MRJ state. In parallel, it establishes that, although the ''pearl-necklace'' model represents the simplest polymer description, it is still able to capture, through the concept of excluded volume, not only the scaling behavior of chain dimensions but even the salient features of the underlying primitive path network. This ability is further substantiated by the data shown in Fig. 2 where the distribution of the entanglement spacing $P(N_e)$ is compared against the exponential-type master curve by Tzoumanekas and Theodorou, based on a stochastic interpretation of entanglement generation in terms of a point process [11(b)]

$$P(N_e) = bc(c-b)^{-1}(e^{-bN_e} - e^{-cN_e}), \quad (3)$$

where b and c are fitting parameters. This formula provided accurate predictions for a wide range of atomistic or coarse-grained polymers [19]. As shown in the main part of Fig. 2, the master curve matches with our results for the $N = 1000$ system at all volume fractions (this holds also for smaller chain lengths, not shown here).

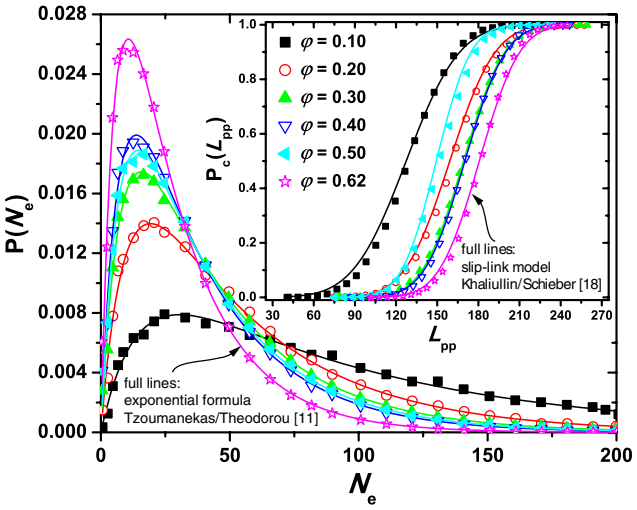

FIG. 2 (color online). Inset: Cumulative probability of the contour length of the primitive path $P_c(L_{\mathrm{PP}})$ for the $N = 1000$ system at various volume fractions (symbols, our data), apparently in agreement with the predictions (lines) according to Eq. (1). Main figure: Distribution of the entanglement spacing N_e for the $N = 1000$ system at various packing densities. Our data (symbols) are excellently captured by the behavior predicted by Eq. (3) (lines).

Next, we perform a geometrical analysis from a new viewpoint based on the concept of knots [20] adopting the technique of [21] for single chains. This technique is based on the identification of the knot group, which is simultaneously more discriminating and easier to calculate than the knot invariants used in the past. Starting from an arbitrary projection of an embedded graph, we generate a sequence of representations, any one of which is a full and complete representation of the knot group. We compare the sequence of representations of any given knot against a previously determined lookup table [22], and if the group of the knot is represented in this table the knot is positively identified. Topological knot theory, however, exclusively deals with knots in closed paths. To apply knotting methodology to linear chains requires us to devise a method to convert a linear polymer into a closed polygon, i.e., by connecting the two ends. Two techniques for doing this are widely used: (i) draw a straight line segment between the two ends, or (ii) starting from the center-of-mass of the chain, project rays outward through the two ends until they intersect a sphere which entirely circumscribes the chain, then connect the two rays using a great circle path between the two intersection points. It was observed that both methods give essentially equivalent scaling behavior of knots. Therefore, for each multichain configuration, we extract the individual chains and convert each one into a closed polygon by connecting its ends with a straight line. The knot state of each resulting polygon is determined using the knot group algorithm [21]. The fraction of knotted chains along with the population of entanglements are displayed in Fig. 3 against packing density.

Surprisingly, both the population of entanglements and knots are found to follow the same scaling laws at all volume fractions. Furthermore, entanglements and knots also exhibit identical crossover concentrations (see inset of Fig. 3). In more detail, we observe the following scaling regimes and corresponding exponents: (a) $0 \leq \varphi \leq \varphi^{*,\mathrm{semi}}$, where knots and entanglements are unaffected (φ^0) by packing density, (b) $\varphi^{*,\mathrm{semi}} \leq \varphi \leq 0.45$ characterized by a scaling exponent of 0.60 ± 0.15, (c) $0.45 \leq \varphi \leq \varphi^{*,\mathrm{conc}}$, where both topological constraints remain practically constant (φ^0), and finally (d) $\varphi^{*,\mathrm{conc}} \leq \varphi \leq \varphi^{\mathrm{MRJ}}$, where a very rapid growth of entanglements and knots is observed characterized by an exponent of 4.0 ± 0.4. There is an interesting side result which deserves being mentioned: The shown knotting probabilities can be cast into the form $P_{\mathrm{knotting}}(N) = 1 - e^{-(N/N_0)^a}$, where (i) the parameter N_0 increases with increasing characteristic ratio C_n (combined Figs. 1–3) but is independent of N, (ii) $N_0 \approx 10^5$ at lowest volume fraction, and (iii) $a \simeq 1.33$ is an empirical factor suggesting a stronger dependence of P_{knotting} on N for linear chains with respect

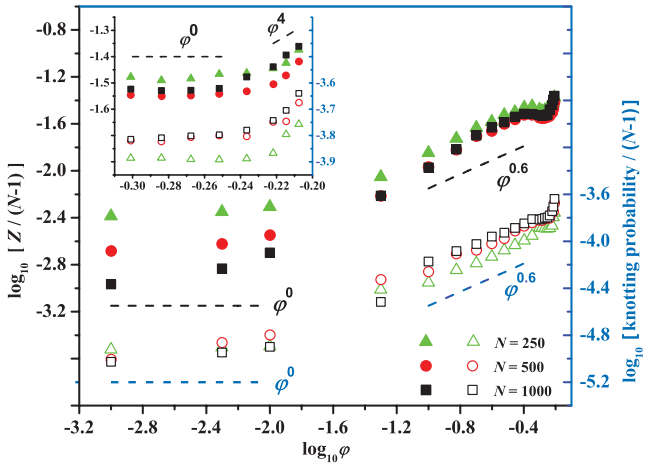

FIG. 3 (color). Average number of entanglements (left axis, filled symbols) and knotting probability per segment (right axis, open symbols) versus packing density. Inset: Zoom into the marginal and concentrated regimes. Lines with characteristic slopes are drawn as guides to the eye.

to ring polymers of tangent hard spheres (for which the above form with features (i) and (ii) but with $a = 1$ had been reported in [23]).

Our finding about the identical scaling of entanglements and knots from the diluted up to the MRJ state is remarkable: although knotting is a purely *intramolecular* characteristic, we find it to be in a very general sense equivalent to entanglements, which are a purely *intermolecular* measure of topological hindrance. It remains to be seen if the analogy also holds for dynamical aspects of entangled polymers. While self-entanglements are seen to play a minor role in characterizing the PP [24], the knot measure contains very different information. In the latter approach, chains can slide past each other at no cost, while no-slip and monotonic path length shrinking is essential [11,13,19] when calculating entanglements.

We acknowledge financial support by the EC through Contract No. NMP3-CT-2005-016375 and allocation of computational resources by CeSViMa (UPM) and CSCS.

*Corresponding author.
nkarayiannis@etsii.upm.es

[1] J. D. Bernal, Nature (London) **188**, 910 (1960).
[2] J. L. Finney, Proc. R. Soc. A **319**, 479 (1970).
[3] S. Torquato, T. M. Truskett, and P. G. Debenedetti, Phys. Rev. Lett. **84**, 2064 (2000).
[4] Z. H. Stachurski, Phys. Rev. Lett. **90**, 155502 (2003).
[5] N. C. Karayiannis and M. Laso, Phys. Rev. Lett. **100**, 050602 (2008).
[6] S. F. Edwards, Proc. Phys. Soc. London **88**, 265 (1966); P. G. de Gennes, *Scaling Concepts in Polymer Physics* (Cornell University, Ithaca, NY, 1980).
[7] N. C. Karayiannis and M. Laso, Macromolecules **41**, 1537 (2008).
[8] M. Doi and S. F. Edwards, *The Theory of Polymer Dynamics* (Clarendon, Oxford, 1988); T. C. B. McLeish, Adv. Phys. **51**, 1379 (2002).
[9] D. W. Mead, R. G. Larson, and M. Doi, Macromolecules **31**, 7895 (1998); S. T. Milner and T. C. B. McLeish, J. Rheol. (N.Y.) **45**, 539 (2001); Y. Masubushi *et al.*, J. Non-Newtonian Fluid Mech. **149**, 87 (2008); J. D. Schieber, J. Chem. Phys. **118**, 5162 (2003).
[10] R. Everaers *et al.*, Science **303**, 823 (2004).
[11] (a) S. Shanbhag and R. G. Larson, Phys. Rev. Lett. **94**, 076001 (2005); (b) C. Tzoumanekas and D. N. Theodorou, Macromolecules **39**, 4592 (2006); (c) K. Foteinopoulou *et al.*, Macromolecules **39**, 4207 (2006); (d) R. S. Hoy and G. S. Grest, Macromolecules **40**, 8389 (2007).
[12] S. Shanbhag and M. Kröger, Macromolecules **40**, 2897 (2007).
[13] M. Kröger, Comput. Phys. Commun. **168**, 209 (2005); M. Kröger, *Models for Polymeric and Anisotropic Liquids* (Springer, Berlin, 2005).
[14] G. J. Fleer *et al.*, *Polymers at Interfaces* (Chapman and Hall, London, 1993).
[15] M. Laso and N. C. Karayiannis, J. Chem. Phys. **128**, 174901 (2008).
[16] M. Daoud *et al.*, Macromolecules **8**, 804 (1975); J. P. Cotton *et al.*, J. Chem. Phys. **65**, 1101 (1976).
[17] N. Uchidaa, G. S. Grest, and R. Everaers, J. Chem. Phys. **128**, 044902 (2008).
[18] R. N. Khaliullin and J. D. Schieber, Phys. Rev. Lett. **100**, 188302 (2008).
[19] K. Kamio, K. Moorthi, and D. N. Theodorou, Macromolecules **40**, 710 (2007).
[20] R. H. Crowell and R. H. Fox, *Introduction to Knot Theory* (Ginn & Co., Boston, MA, 1963).
[21] M. L. Mansfield, J. Chem. Phys. **127**, 244901 (2007).
[22] C. Livingston and J. C. Cha, Table of Knot Invariants, http://www.indiana.edu/~knotinfo.
[23] K. Koniaris and M. Muthukumar, Phys. Rev. Lett. **66**, 2211 (1991).
[24] S. K. Sukumaran *et al.*, J. Polym. Sci. B **43**, 917 (2005); R. S. Hoy and G. S. Grest, Macromolecules **40**, 8389 (2007).